

# SurgSora: Decoupled RGBD-Flow Diffusion Model for Controllable Surgical Video Generation

Tong Chen<sup>1†\*</sup>, Shuya Yang<sup>2\*</sup>, Junyi Wang<sup>3\*</sup>, Long Bai<sup>3†</sup>, Hongliang Ren<sup>3</sup>, and Luping Zhou<sup>1‡</sup>

<sup>1</sup> The University of Sydney, Sydney, Australia

<sup>2</sup> The University of Hong Kong, Hong Kong SAR, China

<sup>3</sup> The Chinese University of Hong Kong, Hong Kong SAR, China  
tche2095@uni.sydney.edu.au, luping.zhou@sydney.edu.au

**Abstract.** Medical video generation has transformative potential for enhancing surgical understanding and pathology insights through precise and controllable visual representations. However, current models face limitations in controllability and authenticity. To bridge this gap, we propose SurgSora, a motion-controllable surgical video generation framework that uses a single input frame and user-controllable motion cues. SurgSora consists of three key modules: the Dual Semantic Injector (DSI), which extracts object-relevant RGB and depth features from the input frame and integrates them with segmentation cues to capture detailed spatial features of complex anatomical structures; the Decoupled Flow Mapper (DFM), which fuses optical flow with semantic-RGB-D features at multiple scales to enhance temporal understanding and object spatial dynamics; and the Trajectory Controller (TC), which allows users to specify motion directions and estimates sparse optical flow, guiding the video generation process. The fused features are used as conditions for a frozen Stable Diffusion model to produce realistic, temporally coherent surgical videos. Extensive evaluations demonstrate that SurgSora outperforms state-of-the-art methods in controllability and authenticity, showing its potential to advance surgical video generation for medical education, training, and research. See our project page for more results: [surgsora.github.io](https://surgsora.github.io).

**Keywords:** Endoscopic Video · Diffusion Model · Video Generation.

## 1 Introduction

Generative artificial intelligence (GAI) has achieved significant success in medical scenarios, including vision-language understanding [36], image restoration [3, 6], data augmentation [37], and medical report generation [20], advancing computer-aided diagnosis and intervention [2, 7]. Recently, researchers have explored video

---

<sup>†</sup> Project Lead; <sup>‡</sup> Corresponding Author.

generation in endoscopic scenarios [18, 23, 40], where realistic dynamic videos offer high-quality resources to support clinician training, medical education, and AI model development. In particular, the controllability of video content—such as the motion of surgical instruments and tissues—becomes crucial for endoscopic surgical video generation [39]. Controllable generation enables dynamic and realistic surgical scenarios based on simple instructions, offering valuable applications in medical training. Furthermore, controllable video generation addresses the scarcity of annotated surgical data, reduces labeling costs, and enhances model generalization, accelerating downstream AI model development and deployment.

General scenarios of controllable video generation using diffusion models have been extensively explored [32], where various control signals—such as motion fields or flow-based deformation modules—are injected through specific parsers to produce videos with desired features and structures [27, 46]. While these approaches enable sophisticated editing of motion patterns, prior works on medical video generation have primarily focused on achieving visually plausible and temporally coherent outputs through effective spatiotemporal modelling [23, 40]. However, the crucial aspect of controllability—specifically for surgical videos—remains largely underexplored. Existing methods, such as Surgeon [8], rely on text descriptions to control video generation, but simple textual input often fails to capture the intricate and dynamic details of surgical procedures, limiting the precision of generated content.

To address this gap, we focus on controllable surgical video generation, where the primary challenge lies in accurately modeling the motion of surgical instruments and tissues based on intuitive user instructions. Given a single surgical image serving as the first frame, we allow users to specify motion directions through a straightforward process akin to direct clicking. This motion direction information is converted into sparse optical flow, which serves as a directive signal for the generation process. To facilitate controllable generation, we propose a novel framework that employs a dual-branch design to extract object-relevant RGB and depth features from the given first frame. These features are then warped using the optical flow data to represent the spatial information of the objects in subsequent frames. Leveraging our proposed multi-information guidance and decoupled flow mapper, our method effectively integrates targeted motion cues, detailed visual features, and object spatial dynamics, enabling the generation of realistic surgical videos with fine-grained motion and precise controllability. This approach not only fills the existing gap in controllable medical video generation but also opens new possibilities for high-fidelity, instruction-driven simulation of surgical scenarios. Our main contributions are summarized as follows.

- We present the first work on motion-controllable surgical video generation using a diffusion model. This novel approach allows fine-grained control (both direction and magnitude) over the motion of surgical instruments and tissues, guided by intuitive motion cues provided by simple clicks.
- We propose the Dual Semantic Injector (DSI), which integrates object-aware RGB-D semantic understanding. The DSI combines appearance (RGB) and

- depth information to better discriminate objects and capture complex anatomical structures, providing an accurate representation of the surgical scene.
- We introduce the Decoupled Flow Mapper (DFM), which effectively fuses optical flow with semantic-RGB-D features at multiple scales. This fusion serves as the guidance conditions for a frozen Stable Video Diffusion model to generate realistic surgical video sequences.
  - We conduct extensive experiments on a public dataset, demonstrating the effectiveness of SurgSora in generating high-quality, motion-controllable surgical videos.

## 2 Related Works

### 2.1 Image-to-Video Generation

Researchers have explored generating videos from images and associated conditions, such as text descriptions [16] or motion control [1]. Controllability remains one of the most significant challenges in I2V generation research. A series of works explore incorporating multiple prompts (e.g., motion, clicks, text, and reference image) to provide more flexible control during video generation [12, 19, 26, 43]. MOFA-Video realizes controllable I2V with sparse motion hints (e.g., trajectories, facial landmarks) via domain-aware MOFA-Adapters to enable precise and diverse motion control across multiple domains [27]. Pix2Gif introduces explicit motion guidance, enabling users to define dynamic elements in the output, thus creating short, loopable animations [21]. Furthermore, ID-Animator [14] and I2V-Adapter [13] insert lightweight adapters into pretrained text-to-video models, employing cross-frame attention mechanisms to achieve efficient and effective I2V generation. In addition, several methods aim to further improve I2V generation performance and maintain high video quality and fidelity. For instance, PhysGen enhances the quality of generative models by using object dynamics and motion derived from physical properties as control conditions [25]. Meanwhile, ConsistI2V improves visual consistency in I2V generation by addressing temporal and spatial inconsistencies, ensuring high visual fidelity [28]. Although extensive research has been conducted on natural and animated scenes, the adaptation of these approaches to medical scenarios remains relatively unexplored and requires further investigation.

### 2.2 Medical Video Generation

Medical video generative models have been widely applied in various scenarios [24], such as ensuring privacy in echocardiogram videos [29], simulating disease progression [5], and editing the Ejection Fraction in ultrasound videos [30]. With advancements in diffusion model families, generalized text-to-video generative models have been explored for controllable generation in diverse medical contexts. For example, Bora, fine-tuned on custom biomedical text-video pairs, can respond to various medical-related text prompts [34]. In the field of endoscopy and surgery, Endora is an unconditional generative model designed as an

endoscopy simulator, capable of replicating diverse endoscopic scenarios for educational purposes [23]. MedSora introduces an advanced video diffusion framework that integrates spatio-temporal Mamba modules, optical flow alignment, and a frequency-compensated video VAE. This framework enhances temporal coherence, reduces computational costs, and preserves critical details in medical videos [40]. Furthermore, Surgen generates realistic surgical videos based on text prompts [8], while Iliash et al. focused on generating videos with instrument-organ interaction with laparoscopic videos [18]. In our work, we aim to enable the model to generate realistic instrument motion in surgical scenes using simple motion cues (i.e., the direction of instrument movement).

### 3 Methodology

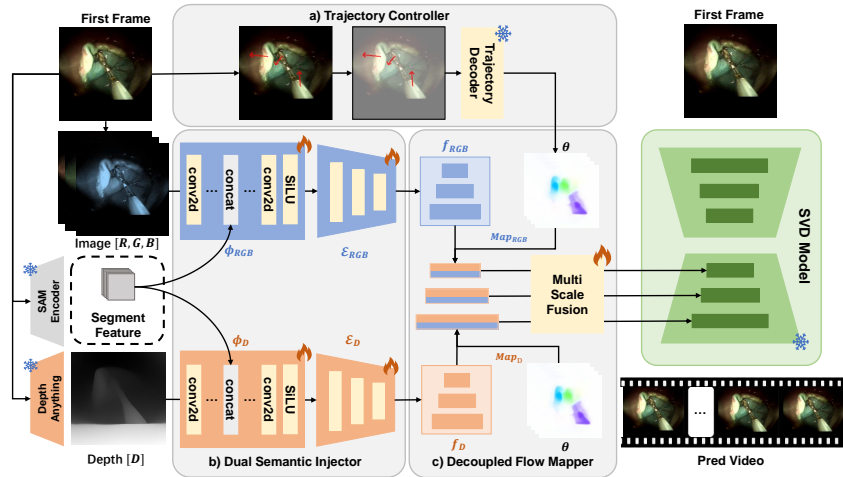


**Fig. 1. The pipeline of SurgSora:** Segment features and depth images are generated from pre-trained models (SAM [22] and DAV2 [42]). **a)** denotes a Trajectory Controller (TC) module, decoding trajectories into sparse optical flow as the condition. **b)** illustrates the Dual Semantic Injector (DSI), which fuses RGB features and depth features with segment features and sends them into encoding blocks, respectively. **c)** Decoupled Flow Mapper (DFM) transforms images and depth features into optical flow separately to get decoupled flow features. The decoupled features are sent into the Multi-Scale Fusion Block for the following generation.

#### 3.1 Overview

Our SurgSora framework, illustrated in Figure 1, comprises three key modules: the Dual Semantic Injector (DSI) introduced in Sec. 3.2, the Decoupled Flow

Mapper (DFM) described in Sec. 3.3, and the Trajectory Controller (TC) module detailed in Sec. 3.4. Our model takes the first image frame  $I_{RGB} \in \mathbb{R}^{3 \times H \times W}$  as input. Based on  $I_{RGB}$ , the corresponding segmentation features  $f_{seg}$  and depth image  $I_D \in \mathbb{D}^{1 \times H \times W}$  are generated from the pretrained Segment Anything Model [22] and the Depth Anything V2 [42]. The segment feature is injected into the RGB and Depth features in the DSI module to extract object-aware image features  $f_{RGB}^r$  and depth features  $f_D^r$  at multi-scales  $r$ . These features are then processed in the DFM module, where the optical flow  $\theta \in \mathbb{O}^{(T-1) \times 2 \times H \times W}$  (with  $T$  as the total number of frames of the generated video), is resized and used to transform  $f_{RGB}^r$  and  $f_D^r$  independently. The transformed features are fused using the Multi-Scale Fusion (MSF) Block at different scales. These multi-scale fused features are then used as conditions for a frozen Stable Video Diffusion (SVD) model to generate the video.

### 3.2 Dual Semantic Injector

Traditional methodologies primarily rely on RGB images as input to create dynamic visual content. While effective in certain applications, this approach suffers from significant limitations in depth perception and scene understanding. Specifically, relying solely on RGB data complicates accurately capturing spatial relationships between objects, leading to deficiencies in visual coherence and object segmentation in generated videos. To address these challenges, we introduce the Dual Semantic Injector (DSI) module, a dual-branch architecture that enhances object awareness by integrating segmentation features into both the RGB and depth feature branches. Unlike traditional methods that depend solely on RGB images, we estimate and incorporate a depth map to provide crucial geometric cues. These cues improve the understanding of spatial relationships between objects and overall scene structure, making it especially beneficial for complex tasks like surgical video synthesis. Furthermore, to better discriminate between objects, object segmentation is leveraged to refine both RGB and depth features.

The segment features  $f_{seg}$  are combined with RGB images  $I_{RGB}$  and depth images  $I_D$  by passing through two separate processors  $\phi_{RGB}$  and  $\phi_D$  for feature extraction and fusion, followed by two separate encoders for further encoding. The Dual Semantic Injector can be formulated as:

$$f^r = \begin{cases} \mathcal{E}_{RGB}^r(\phi_{RGB}(I_{RGB}, f_{seg})), or \\ \mathcal{E}_D^r(\phi_D(I_D, f_{seg})). \end{cases} \quad (1)$$

Recall that the superscript  $r$  indicates different scales of feature maps extracted by the encoders. This design uses a dual encoding method, which synchronizes and harmonizes the enhanced features from RGB and depth channels to optimize the overall representation. The injection of segmentation features enhances the semantic understanding compared with using the original RGB and depth features, significantly improving the discrimination of foreground and background, enhancing depth estimation, and ultimately contributing to more realistic and referenceable video predictions.

### 3.3 Decoupled Flow Mapper

Previous works [27, 31, 46] have demonstrated that the effectiveness of diffusion models can be significantly enhanced by adding additional information encoded into latent spaces. For these reasons, we employ a DFM module that bridges the spatial and sequential information of image and optical features to obtain spatial and temporal features for generating sequential videos. The object-aware RGB and depth features output by the DSI module are spatially transformed by the corresponding resized optical flow, respectively, elaborated as follows.

Let  $f^r \in \mathbb{R}^{C_r \times H_r \times W_r}$  denote the output feature maps of the DSI module from either the RGB or the depth branch and  $f^r(x, y)$  represent the feature at the position  $(x, y)$ . The optical flow  $\theta \in \mathbb{O}^{(T-1) \times 2 \times H \times W}$  is first resized to  $\theta^r \in \mathbb{O}^{(T-1) \times 2 \times H_r \times W_r}$  to match the size of  $f^r$ , and then used to spatially transform  $f^r$  by applying the displacements  $(dx, dy)$  provided in each frame  $\theta_t^r$ , in which  $t \in [0, T)$  represents the current optical frame. The transformation is defined as:

$$x' = x + dx, \quad y' = y + dy. \quad (2)$$

Here,  $dx$  and  $dy$  represent the displacements in the horizontal and vertical directions, respectively. Bilinear interpolation is used to estimate the updated pixel values at the new displacements  $(dx, dy)$ . The mapping procedure is given by:

$$\hat{f}^r(x', y') = \text{Interpolate}(f^r(x, y)). \quad (3)$$

Depth information typically captures geometry and spatial structure, while RGB information focuses on appearance and texture. To effectively leverage these complementary properties, we employ a decoupled-mapping method to independently spatially transform and extract frame features from the depth and RGB streams, and then integrate them via a Multi-Scale Fusion Block.

**Multi-Scale Fusion Block (MSF)** fuses the optical-flow-transformed RGB and depth features by concatenating them at different scales and then fusing them by two 3D convolution blocks and an activation block. The fusion process is expressed as:

$$\check{f}_{fuse}^r = \text{SiLU}(\text{Conv3d}(\text{Conv3d}(\text{CONCAT}(\hat{f}_{RGB}^r, \hat{f}_D^r)))). \quad (4)$$

The fused feature  $\check{f}_{fuse}^r$  is then used to assist a frozen Stable Video Diffusion Model for conditional video generation.

In sum, the integration of optical flow information enhances temporal continuity between frames, improving the smoothness and visual coherence of the generated videos. It enables the model to accurately capture scene dynamics and interactions, effectively interpreting complex motion. By fusing information from multiple modalities, the model achieves a more comprehensive understanding of scene depth and structure, maintaining visual authenticity while adapting to subtle changes. This multimodal strategy not only elevates video quality but also enriches detail and realism, ensuring a more accurate and dynamic representation of the scene.

### 3.4 Trajectory Controller

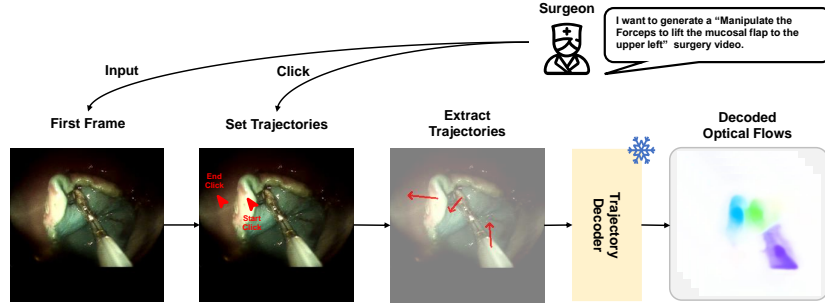


**Fig. 2.** Workflow of Trajectory Controller (TC) module: First, the surgeon inputs the required surgical image as the first frame. Then, the surgeon clicks the image again to set the trajectories. The trajectories are sent into the Trajectories Decoder to get sparse optical for the following steps.

Surgical videos require more precision compared with natural videos, and generation with a single image makes it more difficult and non-referencable. Therefore, the Trajectory Controller (TC) is employed to enable custom trajectories as input for conditional motion generation. The pipeline of our TC module is shown in Figure 2, which employs a pre-trained trajectory decoder from [45]. The surgeon inputs the first frame image and then clicks to set trajectories. The trajectories and image will be encoded separately, concatenated together, and then decoded by the trajectory decoder into optical flows as a condition to guide the following generation. By involving the TC module, the quality of the generated video will be more referencable and convenient for generating customized surgical videos.

## 4 Experiment

### 4.1 Dataset and implementation details

We utilize the publicly available CoPESD dataset [38], which was collected from 20 videos using both conventional endoscopic submucosal dissection (ESD) and the DREAMS system [10], performed on in-vivo porcine models. The videos were recorded at a frame rate of 30 Hz with an original resolution of  $1920 \times 1080$ , which was cropped to  $1300 \times 1024$ . After an expert surgeon provided temporal annotations of ESD activities, video segments corresponding to submucosal dissection were separately extracted. We extract 21-frame video clips from the datasets, then resize them into  $256 \times 197$  resolution and pad them to  $256 \times 256$

resolution as the training and testing set. We employ the AdamW optimizer with a constant learning rate  $2 \times 10^{-5}$  for training. We set the batch size as 4 and trained the model on two RTX A6000 GPUs for 20000 iterations of training.

## 4.2 Comparison Methods and Evaluation Metrics

We compare performance against advanced video generation models on CoPESD datasets, including two unconditional generative video models, Endora [23] and StyleGAN-V [33]; and a conditional generative video model, MOFA-Video [27].

To evaluate the quality of the generated videos, we employ Fréchet Video Distance (FVD) [35] and Content-Debiased Fréchet Video Distance (CD-FVD) [11] to evaluate temporal consistency and the overall realism of the video, and Fréchet Inception Distance (FID) [15] and Inception Score (IS) [4] to evaluate the realism, fidelity, and diversity of individual frames. In addition, we also measure the frame consistency [9] by calculating the average CLIP cosine similarity of two consecutive frames. Meanwhile, for conditional video generation, we follow traditional pixel- or local-level video assessment metrics, including Peak Signal-to-Noise Ratio (PSNR) [17] and Structural Similarity Index (SSIM) [41], to assess the content and structural quality of the generated video against the ground truth. Furthermore, we include optical flow evaluation metrics, specifically the F1-epe and F1-all scores, to assess the consistency between the optical flow of the generated video and the given optical flow.

## 4.3 Results

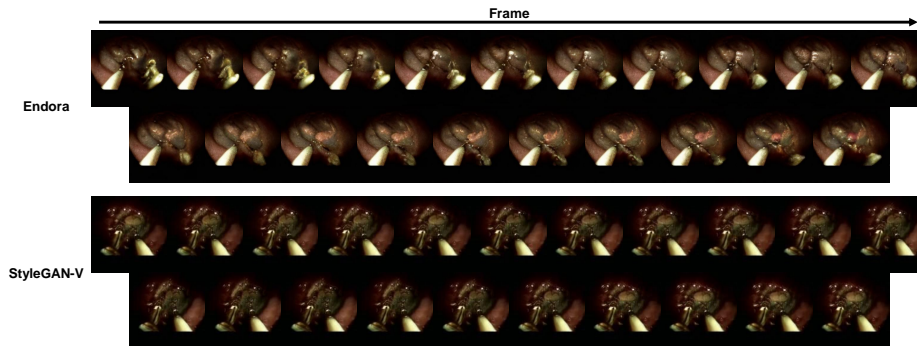


**Fig. 3.** Comparison of unconditional generation results trained on CoPESD dataset: Both Endora [23] and StyleGAN-V [33] models generated videos with different levels of noticeable gaps compared with the real surgical scene (tissues and instruments).

**Video Generation Evaluation and Visualization** Table 1 and Table 2 quantitatively compare the performance of SurgSora with existing methods. The



**Table 1.** Quantitative Comparisons on CoPESD Dataset [38]. The comparison contains both video consistency and video content qualities.

| Models                 | Frame Consistency $\uparrow$ | FVD $\downarrow$ | CD-FVD $\downarrow$ | FID $\downarrow$ | IS $\uparrow$ |
|------------------------|------------------------------|------------------|---------------------|------------------|---------------|
| Endora [23]            | 97.51%                       | 1146.54          | 1289.59             | 205.93           | 2.239         |
| StyleGAN-V [44]        | 98.02%                       | 857.16           | 980.11              | 166.03           | 2.267         |
| MOFA-Video [27]        | 95.59%                       | 671.66           | 692.44              | 96.31            | 2.685         |
| <b>SurgSora (Ours)</b> | <b>98.70%</b>                | <b>395.65</b>    | <b>535.95</b>       | <b>87.94</b>     | <b>3.278</b>  |

**Table 2.** Quantitative Comparisons on CoPESD Dataset [38]: This table evaluates conditionally generated video and optical flow qualities.

| Models                 | Video           |                 | Optical Flow        |                     |
|------------------------|-----------------|-----------------|---------------------|---------------------|
|                        | PSNR $\uparrow$ | SSIM $\uparrow$ | F1-epe $\downarrow$ | F1-all $\downarrow$ |
| MOFA-Video [27]        | 19.06           | 48.28%          | 0.2620              | 265.54              |
| <b>SurgSora (Ours)</b> | <b>20.71</b>    | <b>55.94%</b>   | <b>0.1477</b>       | <b>149.89</b>       |

two unconditional video generative models, Endora [23] and StyleGAN-V [33] take random noise as the input, while the conditional video generative models, MOFA-Video [27] and our SurgSora take the first image frame as the input. Here, to facilitate the comparison with the ground-truth videos, we employ the optical flows estimated from the ground-truth video as the trajectory control.

As can be seen from Table 1, our framework exhibits the highest Frame Consistency at 98.70%, which is a modest improvement over StyleGAN-V’s 98.02% and a more pronounced leap from Endora’s 97.51%. This indicates our model’s ability to maintain uniformity and temporal stability across video frames more effectively. More importantly, in terms of video quality metrics, our method achieves the lowest FVD at 395.65 as compared to StyleGAN-V and Endora, which record FVDs of 857.16 and 1146.54, respectively. The CD-FVD, which assesses content and dynamics in video synthesis, further underscores our method’s effectiveness with a score of 535.95, markedly better than the closest method, MOFA-Video [27] at 671.66. Furthermore, our approach achieves the best FID of 87.94, improving upon MOFA-Video’s 96.31 and significantly outperforming Endora’s 205.93. This suggests that the videos generated by SurgSora are visually closer to authentic videos, thereby capturing the nuances of video content with greater fidelity. SurgSora outperforms the IS score (3.278) among all, which indicates better-generated frames in terms of objectness and diversity.

Moreover, for conditional generation, as shown in Table 2, SurgSora outperforms MOFA-Video with scores of 20.71 dB in PSNR and 55.94% in SSIM compared to MOFA-Video (19.06 dB and 48.28%), which confirms our model’s superior capacity in preserving generation quality and structural similarity. Notably, we evaluate the model’s ability to adhere to trajectory control by comparing the given optical flow with the optical flow extracted from the generated

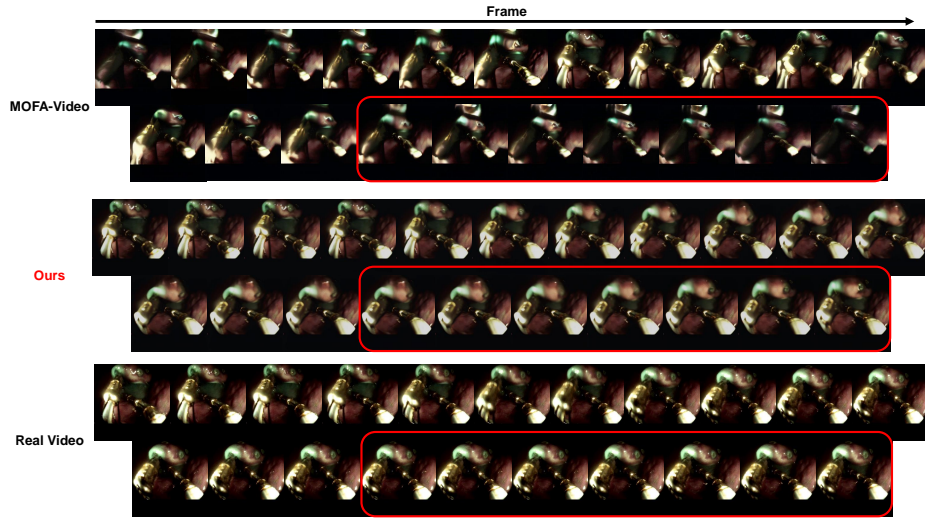


**Fig. 4.** Comparison of conditional generation results trained on CoPESD dataset: Generated video by ours retains most of the authenticity of the real video. The video generated by MOFA-Video [27] has a serious distortion at the end of the video.

video. Our SurgSora framework consistently demonstrates superior accuracy in following the specified generation instructions.

Visual comparisons are given in Figure 3 for unconditional generation and Figure 4 for conditional generation. Unconditionally generated videos from both Endora [23] and StyleGAN-V [33] do not conform to reality in terms of the generation of scenes and instruments, which cannot accurately reflect real medical situations. Conditionally generated video by MOFA-Video [27] involves serious frame distortion at the end of the video. Our SurgSora-generated video maintains most of the real video’s authenticity, further showing its superior performance.

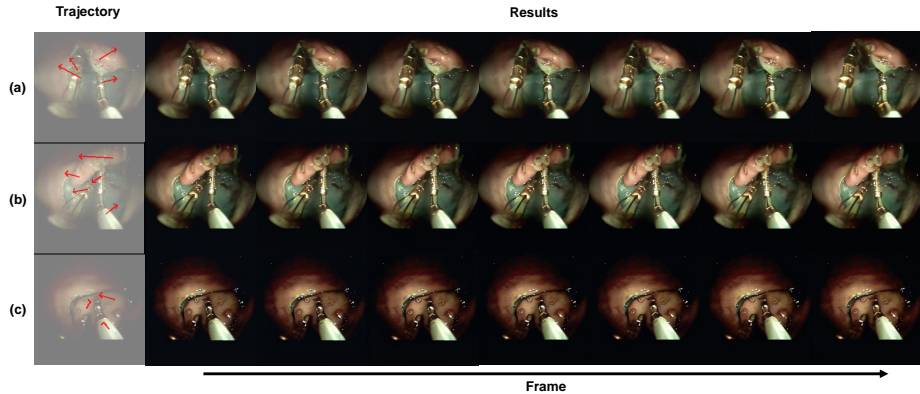


**Fig. 5.** The quantitative results of our SurgSora with different trajectory conditions.

**Table 3.** Ablation experiments of our SurgSora on the CoPESD Dataset [38]. To observe the performance changes, we (i) remove the Segment Feature, (ii) degenerate the depth branch, and (iii) discard the Multi-Scale Fusion Block.

| Segment Feature | Depth Branch | Multi-Scale Fusion | Frame Consistency $\uparrow$ | FVD $\downarrow$ | CD-FVD $\downarrow$ | FID $\downarrow$ | IS $\uparrow$ | PSNR $\uparrow$ | SSIM $\uparrow$ |
|-----------------|--------------|--------------------|------------------------------|------------------|---------------------|------------------|---------------|-----------------|-----------------|
| ✓               | ✗            | —                  | 98.08%                       | 442.66           | 584.46              | 90.97            | 3.199         | 20.47           | 53.59%          |
| ✗               | ✓            | ✗                  | 96.99%                       | 510.11           | 782.51              | 115.72           | 2.586         | 19.49           | 54.59%          |
| ✗               | ✓            | ✓                  | 98.35%                       | 479.13           | 624.63              | 88.85            | 3.076         | 17.59           | 53.18%          |
| ✓               | ✓            | ✗                  | 97.53%                       | 422.06           | 603.34              | 88.54            | 3.270         | 20.64           | 51.33%          |
| ✓               | ✓            | ✓                  | <b>98.70%</b>                | <b>395.65</b>    | <b>535.95</b>       | <b>87.94</b>     | <b>3.278</b>  | <b>20.71</b>    | <b>55.94%</b>   |

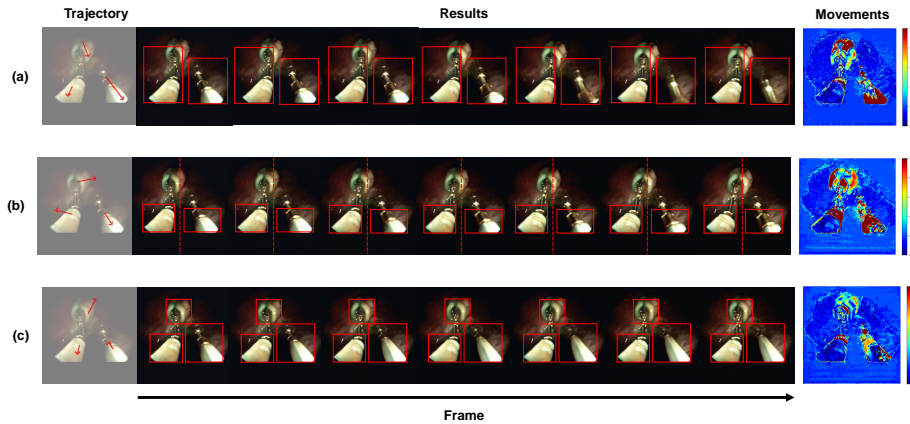


**Fig. 6.** The quantitative results of our SurgSora using different trajectory conditions: We calculated the difference between the first and last frames and visualized it as a heatmap, where red means high movements and blue represents low movements. Zoom in to see the details.

**Customize Trajectory Video Generation** To address the effectiveness of our Trajectory Controller block, we generate a few demos by using the TC module. Figure 5 shows videos generated from varying surgical image trajectories, clearly depicting the dynamic movement and transformation of the objects within the images in accordance with the specified trajectories. Further demonstrating the module’s capacity for precise control, we generated distinct trajectories within the same image, as presented in Figure 6. We manipulated tissues and instruments to move in designated directions, and the visual results showed that objects along the set paths moved without noticeable distortion. The heatmap indicates that devices have undergone obvious changes according to the trajectory requirements while maintaining the background unchanged. These outcomes validate the high performance and accuracy of our module in controlling and generating detailed movement in medical imagery.

**Ablation Study** We conduct ablation studies on our SurgSora model using the CoPESD Dataset [38] to demonstrate the contribution of each component, with results summarized in Table 3. Comparing Rows 3 and 5 in the Table, disabling the segment feature while retaining the depth branch and Multi-Scale Fusion (MSF) block leads to a performance drop, with FVD/CD-FVD increasing from 395.65/535.95 to 479.13/624.63, highlighting the segment feature’s role in enhancing visual coherence and temporal consistency. Comparing Rows 2 and 3, further removing the MSF block results in a substantial decline, with Frame Consistency dropping to 96.99% and FVD/CD-FVD increasing significantly to 510.11/782.51, indicating the depth branch’s importance in integrating spatial information. Comparing Rows 4 and 5, when the MSF block alone is disabled but the segment feature and depth branch remain active, the performance degradation is less severe, with Frame Consistency at 97.53% and moderate increases in FVD/CD-FVD (422.06/603.34), showing that the MSF block enhances feature fusion but the segment feature and depth branch remain crucial. Direct use of decoupled-flow features produces the worst SSIM score (51.33%), suggesting poor structural preservation, which improves with the depth branch but still incurs computational complexity and lower performance. The addition of the MSF block resolves this issue by aligning the decoupled features with the overall framework, significantly improving metrics. In Row 5, integrating all three components—segment feature, depth branch, and MSF block—our complete SurgSora achieves the best performance, demonstrating their collective effectiveness in enhancing video quality, structural consistency, and temporal coherence.

## 5 Limitation

The accuracy and authenticity of videos are particularly important in the medical field. Moreover, the complexity of medical videos is much higher than that of general video content, containing complex dynamic structures and rich details. SurgSora has been evaluated on specific datasets, but its ability to generalize across surgical scenarios and different types of surgeries still needs to be questioned. Besides that, generating long clips requires the model to sustain narrative coherence and visual consistency, which remains challenging due to accumulating errors and drifts in the generated content over time. The model’s current capabilities may not fully account for the dynamic and unpredictable nature of live surgeries, where multiple instruments and varying anatomical structures interact in complex ways. This limitation affects the model’s utility in training and planning, where understanding these interactions is crucial. Addressing these limitations requires advancements in computational strategies and more robust adaptability of the model to diverse medical contexts. By overcoming these challenges, medical video generation technology can significantly improve, offering more reliable tools for medical training and procedural planning.

## 6 Conclusion

In this study, we propose SurgSora, a customized RGBD-flow-guided conditional diffusion video model. SurgSora incorporates a separate depth branch, the Dual Semantic Injector (DSI), which increases object semantics information for dual features, and the Decoupled Flow Mapper (DFM) to provide a more suitable and richer feature representation for the Stable Video Diffusion model. Quantitative and qualitative experiments demonstrate superior performance in medical video generation and the ability to generate reasonable videos with simple trajectories. SurgSora provides a brand new view on the medical video generation field. Future works will focus on high-quality long medical clip generation and multimodal conditional medical video generation.

## References

1. Ardino, P., De Nadai, M., Lepri, B., Ricci, E., Lathuilière, S.: Click to move: Controlling video generation with sparse motion. In: Proceedings of the IEEE/CVF International Conference on Computer Vision. pp. 14749–14758 (2021)
2. Bai, L., Chen, T., Tan, Q., Nah, W.J., Li, Y., He, Z., Yuan, S., Chen, Z., Wu, J., Islam, M., et al.: Endouic: Promptable diffusion transformer for unified illumination correction in capsule endoscopy. In: International Conference on Medical Image Computing and Computer-Assisted Intervention. pp. 296–306. Springer (2024)
3. Bai, L., Chen, T., Wu, Y., Wang, A., Islam, M., Ren, H.: Llcaps: Learning to illuminate low-light capsule endoscopy with curved wavelet attention and reverse diffusion. In: International Conference on Medical Image Computing and Computer-Assisted Intervention. pp. 34–44. Springer (2023)
4. Barratt, S., Sharma, R.: A note on the inception score. arXiv preprint arXiv:1801.01973 (2018)
5. Cao, X., Liang, K., Liao, K.D., Gao, T., Ye, W., Chen, J., Ding, Z., Cao, J., Rehg, J.M., Sun, J.: Medical video generation for disease progression simulation. arXiv preprint arXiv:2411.11943 (2024)
6. Chen, T., Lyu, Q., Bai, L., Guo, E., Gao, H., Yang, X., Ren, H., Zhou, L.: Lightdiff: Surgical endoscopic image low-light enhancement with t-diffusion. In: International Conference on Medical Image Computing and Computer-Assisted Intervention. pp. 369–379. Springer (2024)
7. Chen, Y., Esmailzadeh, P.: Generative ai in medical practice: in-depth exploration of privacy and security challenges. *Journal of Medical Internet Research* **26**, e53008 (2024)
8. Cho, J., Schmidgall, S., Zakka, C., Mathur, M., Kaur, D., Shad, R., Hiesinger, W.: Surgen: Text-guided diffusion model for surgical video generation. arXiv preprint arXiv:2408.14028 (2024)
9. Esser, P., Chiu, J., Atighehchian, P., Granskog, J., Germanidis, A.: Structure and content-guided video synthesis with diffusion models. In: Proceedings of the IEEE/CVF International Conference on Computer Vision. pp. 7346–7356 (2023)
10. Gao, H., Yang, X., Xiao, X., Zhu, X., Zhang, T., Hou, C., Liu, H., Meng, M.Q.H., Sun, L., Zuo, X., et al.: Transendoscopic flexible parallel continuum robotic mechanism for bimanual endoscopic submucosal dissection. *The International Journal of Robotics Research* **43**(3), 281–304 (2024)

11. Ge, S., Mahapatra, A., Parmar, G., Zhu, J.Y., Huang, J.B.: On the content bias in fréchet video distance. In: Proceedings of the IEEE/CVF Conference on Computer Vision and Pattern Recognition (CVPR) (2024)
12. Gong, L., Zhu, Y., Li, W., Kang, X., Wang, B., Ge, T., Zheng, B.: Atomovideo: High fidelity image-to-video generation. arXiv preprint arXiv:2403.01800 (2024)
13. Guo, X., Zheng, M., Hou, L., Gao, Y., Deng, Y., Ma, C., Hu, W., Zha, Z., Huang, H., Wan, P., et al.: I2v-adapter: A general image-to-video adapter for video diffusion models. arXiv preprint arXiv:2312.16693 (2023)
14. He, X., Liu, Q., Qian, S., Wang, X., Hu, T., Cao, K., Yan, K., Zhang, J.: Id-animator: Zero-shot identity-preserving human video generation. arXiv preprint arXiv:2404.15275 (2024)
15. Heusel, M., Ramsauer, H., Unterthiner, T., Nessler, B., Hochreiter, S.: Gans trained by a two time-scale update rule converge to a local nash equilibrium. *Advances in neural information processing systems* **30** (2017)
16. Hu, Y., Luo, C., Chen, Z.: Make it move: controllable image-to-video generation with text descriptions. In: Proceedings of the IEEE/CVF Conference on Computer Vision and Pattern Recognition. pp. 18219–18228 (2022)
17. Huynh-Thu, Q., Ghanbari, M.: Scope of validity of psnr in image/video quality assessment. *Electronics letters* **44**(13), 800–801 (2008)
18. Iliash, I., Allmendinger, S., Meissen, F., Köhl, N., Rückert, D.: Interactive generation of laparoscopic videos with diffusion models. In: MICCAI Workshop on Deep Generative Models. pp. 109–118. Springer (2024)
19. Jiang, Y., Wu, T., Yang, S., Si, C., Lin, D., Qiao, Y., Loy, C.C., Liu, Z.: Video-booth: Diffusion-based video generation with image prompts. In: Proceedings of the IEEE/CVF Conference on Computer Vision and Pattern Recognition. pp. 6689–6700 (2024)
20. Jin, H., Che, H., Lin, Y., Chen, H.: Promptmrg: Diagnosis-driven prompts for medical report generation. In: Proceedings of the AAAI Conference on Artificial Intelligence. vol. 38, pp. 2607–2615 (2024)
21. Kandala, H., Gao, J., Yang, J.: Pix2gif: Motion-guided diffusion for gif generation. arXiv preprint arXiv:2403.04634 (2024)
22. Kirillov, A., Mintun, E., Ravi, N., Mao, H., Rolland, C., Gustafson, L., Xiao, T., Whitehead, S., Berg, A.C., Lo, W.Y., et al.: Segment anything. In: Proceedings of the IEEE/CVF International Conference on Computer Vision. pp. 4015–4026 (2023)
23. Li, C., Liu, H., Liu, Y., Feng, B.Y., Li, W., Liu, X., Chen, Z., Shao, J., Yuan, Y.: Endora: Video generation models as endoscopy simulators. In: International Conference on Medical Image Computing and Computer-Assisted Intervention. pp. 230–240. Springer (2024)
24. Li, L., Qiu, J., Saha, A., Li, L., Li, P., He, M., Guo, Z., Yuan, W.: Artificial intelligence for biomedical video generation. arXiv preprint arXiv:2411.07619 (2024)
25. Liu, S., Ren, Z., Gupta, S., Wang, S.: Physgen: Rigid-body physics-grounded image-to-video generation. In: European Conference on Computer Vision. pp. 360–378. Springer (2025)
26. Ma, Y., He, Y., Wang, H., Wang, A., Qi, C., Cai, C., Li, X., Li, Z., Shum, H.Y., Liu, W., et al.: Follow-your-click: Open-domain regional image animation via short prompts. arXiv preprint arXiv:2403.08268 (2024)
27. Niu, M., Cun, X., Wang, X., Zhang, Y., Shan, Y., Zheng, Y.: Mofa-video: Controllable image animation via generative motion field adaptations in frozen image-to-video diffusion model. arXiv preprint arXiv:2405.20222 (2024)

28. Ren, W., Yang, H., Zhang, G., Wei, C., Du, X., Huang, W., Chen, W.: Consisti2v: Enhancing visual consistency for image-to-video generation. arXiv preprint arXiv:2402.04324 (2024)
29. Reynaud, H., Meng, Q., Dombrowski, M., Ghosh, A., Day, T., Gomez, A., Leeson, P., Kainz, B.: Echonet-synthetic: Privacy-preserving video generation for safe medical data sharing. In: International Conference on Medical Image Computing and Computer-Assisted Intervention. pp. 285–295. Springer (2024)
30. Reynaud, H., Vlontzos, A., Dombrowski, M., Gilligan Lee, C., Beqiri, A., Leeson, P., Kainz, B.: D’artagnan: Counterfactual video generation. In: International Conference on Medical Image Computing and Computer-Assisted Intervention. pp. 599–609. Springer (2022)
31. Rombach, R., Blattmann, A., Lorenz, D., Esser, P., Ommer, B.: High-resolution image synthesis with latent diffusion models. In: Proceedings of the IEEE/CVF conference on computer vision and pattern recognition. pp. 10684–10695 (2022)
32. Shi, X., Huang, Z., Wang, F.Y., Bian, W., Li, D., Zhang, Y., Zhang, M., Cheung, K.C., See, S., Qin, H., et al.: Motion-i2v: Consistent and controllable image-to-video generation with explicit motion modeling. In: ACM SIGGRAPH 2024 Conference Papers. pp. 1–11 (2024)
33. Skorokhodov, I., Tulyakov, S., Elhoseiny, M.: Stylegan-v: A continuous video generator with the price, image quality and perks of stylegan2. In: Proceedings of the IEEE/CVF conference on computer vision and pattern recognition. pp. 3626–3636 (2022)
34. Sun, W., You, X., Zheng, R., Yuan, Z., Li, X., He, L., Li, Q., Sun, L.: Bora: Biomedical generalist video generation model. arXiv preprint arXiv:2407.08944 (2024)
35. Unterthiner, T., Van Steenkiste, S., Kurach, K., Marinier, R., Michalski, M., Gelly, S.: Towards accurate generative models of video: A new metric & challenges. arXiv preprint arXiv:1812.01717 (2018)
36. Wang, G., Bai, L., Nah, W.J., Wang, J., Zhang, Z., Chen, Z., Wu, J., Islam, M., Liu, H., Ren, H.: Surgical-ivlm: Learning to adapt large vision-language model for grounded visual question answering in robotic surgery. arXiv preprint arXiv:2405.10948 (2024)
37. Wang, G., Bai, L., Wu, Y., Chen, T., Ren, H.: Rethinking exemplars for continual semantic segmentation in endoscopy scenes: Entropy-based mini-batch pseudo-replay. *Computers in Biology and Medicine* **165**, 107412 (2023)
38. Wang, G., Xiao, H., Gao, H., Zhang, R., Bai, L., Yang, X., Li, Z., Li, H., Ren, H.: Copesd: A multi-level surgical motion dataset for training large vision-language models to co-pilot endoscopic submucosal dissection. arXiv preprint arXiv:2410.07540 (2024)
39. Wang, S., Du, Y., Guo, X., Pan, B., Qin, Z., Zhao, L.: Controllable data generation by deep learning: A review. *ACM Computing Surveys* **56**(9), 1–38 (2024)
40. Wang, Z., Zhang, L., Wang, L., Zhu, M., Zhang, Z.: Optical flow representation alignment mamba diffusion model for medical video generation. arXiv preprint arXiv:2411.01647 (2024)
41. Wang, Z., Bovik, A.C., Sheikh, H.R., Simoncelli, E.P.: Image quality assessment: from error visibility to structural similarity. *IEEE transactions on image processing* **13**(4), 600–612 (2004)
42. Yang, L., Kang, B., Huang, Z., Zhao, Z., Xu, X., Feng, J., Zhao, H.: Depth anything v2. arXiv preprint arXiv:2406.09414 (2024)

43. Yang, S., Li, H., Wu, J., Jing, M., Li, L., Ji, R., Liang, J., Fan, H., Wang, J.: Megactor- $\sigma$ : Unlocking flexible mixed-modal control in portrait animation with diffusion transformer. arXiv preprint arXiv:2408.14975 (2024)
44. Yu, S., Tack, J., Mo, S., Kim, H., Kim, J., Ha, J.W., Shin, J.: Generating videos with dynamics-aware implicit generative adversarial networks. In: International Conference on Learning Representations (2022), <https://openreview.net/forum?id=Czsdv-S4-w9>
45. Zhan, X., Pan, X., Liu, Z., Lin, D., Loy, C.C.: Self-supervised learning via conditional motion propagation. In: Proceedings of the IEEE/CVF Conference on Computer Vision and Pattern Recognition. pp. 1881–1889 (2019)
46. Zhang, L., Rao, A., Agrawala, M.: Adding conditional control to text-to-image diffusion models. In: Proceedings of the IEEE/CVF International Conference on Computer Vision. pp. 3836–3847 (2023)